Robotica (2019) volume 37, pp. 708–728. © Cambridge University Press 2018
doi:10.1017/S0263574718001273

Inverse Dynamics of a 3-P[2(US)] Translational Parallel Robot

Mahmood Mazare†, Mostafa Taghizadeh†* and M. Rasool Najafi†‡

† *School of Mechanical Engineering, Shahid Beheshti University, Tehran, Iran*
E-mail: m_mazare@sbu.ac.ir
‡ *Department of Mechanical Engineering, University of Qom, Qom, Iran*
E-mail: mr.najafi@gom.ac.ir

(Accepted November 03, 2018. First published online: December 26, 2018)

SUMMARY
In this paper, a type of parallel robot with three translational degrees of freedom is studied. Inverse and forward kinematic equations are extracted for position and velocity analyses. The dynamic model is derived by Lagrange's approach and the principle of virtual work and related computational algorithms implementing inverse and forward dynamics are presented. Furthermore, some numerical simulations are performed using the kinematic and dynamic models in which the results show good agreement with expected qualitative behavior of the mechanism. Comparisons with the results of work-energy and impulse-momentum methods quantitatively verify the validity of the derived equations of motion. Also, a relative computational effectiveness is observed in implementation of virtual work model via the simulations.

KEYWORDS: Kinematic modeling; Parallel robot; Dynamic modeling; Constrained system equations; Virtual work.

1. Introduction

In the past few decades, parallel robotic manipulators have attracted the attention of industry and academia. In these mechanisms, mobile and fixed platforms are connected by several branches with fixed or variable lengths. Compared to serial robots, parallel robots have special features such as high rigidity, more stable performance, high dynamic load capacity, and better position accuracy which have different applications such as CNC machining, medical, and so on.[1] Because of the above-mentioned benefits, extensive research is being done on the parallel robotic manipulators such as kinematic and workspace analysis,[2] dynamic modeling,[3] and parameters identification.[4]

Parallel robots have their own limitations such as small and complex workspace, combination of translational and rotational workspace into each other, and clearance in joints.[5] Also, complex dynamics and forward kinematics of parallel robots require a very sophisticated real-time control of these robots.[6]

Closed loop chain and kinematic constraints have made dynamic modeling of these mechanisms complicated. In order to derive the dynamic equations of a parallel robot, several methods can be used such as the Newton–Euler, Lagrange, Kane, and Gibbs–Apple methods. Do and Yang,[7] Reboulet and Berthomieu,[8] and Ji[9] derived the dynamic model of Stewart platform based on the Newton–Euler method. Ji also considered the effects of links inertia in dynamic modeling. Xingwei *et al.*[10] performed dynamic modeling of a CPPPMS parallel robot in which the actuator dynamics was also considered. Dynamic evaluation of a type of parallel robot has been done in ref. [11] using several

* Corresponding author. E-mail: mo_taghizadeh@sbu.ac.ir

https://doi.org/10.1017/S0263574718001273 Published online by Cambridge University Press

performance indices. Dynamic analysis of a planar parallel robot considering singularities and different payloads is performed by Özdemir.[12] Dynamic performance analysis of an X4 high-speed pick-and-place parallel robot is also presented in ref. [13] in which a new index is proposed to indicate the acceleration consistency of each limb of the parallel robot. Dynamic model of redundant hybrid manipulators connected in series by three or more different parallel manipulators with linear active legs has been proposed by Lu *et al.*[14] in which dynamical equations are derived using unified recursive dynamic formulae.

Many other methods which use the principles of classical mechanics have been applied in the literature to model the dynamics of parallel robots, such as virtual work principle,[15,16] screw theory,[17] recursive matrix method,[18] and Hamilton principle.[19] Dynamic modeling of a Stewart-based hybrid parallel robot was proposed in ref. [20] in which the model uses recursive matrix relations. In ref. [21], kinematic analysis of a 3-PRS parallel manipulator is studied and inverse dynamic modeling is analyzed based on Lagrange formulation and principle of virtual work.

In this paper, dynamic modeling of a 3-DOF (degrees of freedom) translational parallel robot, 3-[P2(US)], is performed. This robot was previously introduced by the authors in ref. [22]. Based on kinematic analysis for constrained systems, Jacobian matrix and Jacobian of constraints are derived. Then, dynamic modeling of this mechanism is performed via Lagrange method which is a very important step in robot control. Constraint equations of motion consist of six Lagrange equations containing Lagrange multipliers and three constraint equations all nonlinear in terms of generalized coordinates of the system. Eliminating Lagrange multipliers, the reduced dynamic equations of the robot are represented as a partitioned matrix form.

Since the main objective of this study is to derive the dynamic model of the 3-[P2(US)] parallel robot for the first time, the equations of motion are also derived using the principle of virtual work. This model includes some simplicity in comparison with the Lagrange model. Three simulations are performed to indicate the qualitative behavior of the mechanism under the applied actuator forces. Comparisons of the results of the dynamic model with the results of work–energy and impulse–momentum theorems verify validity of the derived equations of motions quantitatively.

It should be noted that this mechanism is a modified design of delta-type robots. Usual architecture of delta robots such as 3-[R2(US)] delta robot which is actuated via the revolute joints has less ability to apply enough force on the end-effector. Also, the 3-PUU delta robot has less resistance against rotation of the end-effector at the universal joints. The aim of proposed 3-[P2(US)] architecture is utilization of pneumatic actuators in order to overcome reactions on the end-effector and also to create more resistance against rotation via two spherical joints in each limb.

The main contributions of this paper are:

(1) Deriving the dynamic model of the modified architecture of delta robot.
(2) Study of the effect of the simplifying assumption (replacing rotational inertia of the connecting rods with concentrated masses) on motion simulation of the mechanism.
(3) Investigation of relative simplicity and less computational effort in the model derived by the principle of virtual work.

The remainder of this paper is organized as follows. In Section 2, geometry of the 3-[P2(US)] parallel robot is introduced. In Sections 3 and 4, the kinematic and dynamic models of the proposed mechanism are derived. Verification of the derived model, utilizing a software simulation, is presented in Section 5. Results of simulations are reported in Section 6 and finally, conclusion is drawn in Section 7.

2. Geometry of the Parallel Robot

The studied mechanism is constituted of a fixed platform at the top, a mobile platform (end-effector) at the bottom, and three limbs. Each of the limbs is constituted of two parallel connecting rods attached to a slider at the top via universal joints and attached to the end-effector at the bottom via spherical joints. Each slider is connected to the fixed platform by a prismatic joint. Prismatic joints are actuated by linear actuators. In Fig. 1, the assembled robot is demonstrated.

Schematic presentation of the robot mechanism is depicted in Fig. 2. On each limb, two universal joints are connected to two spherical joints by two parallel rods. The architecture of the mechanism is called 3-[P2(US)]. In order to prevent rotational motion of end-effector, parallelogram linkages

https://doi.org/10.1017/S0263574718001273 Published online by Cambridge University Press

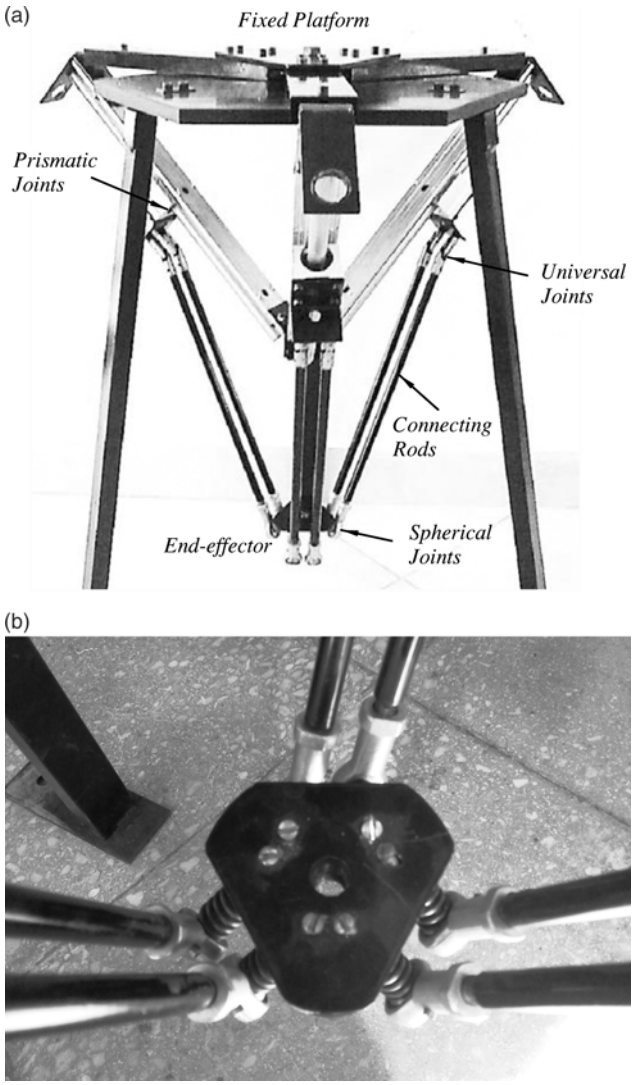


Fig. 1. (a) Prototype of 3-[P2(US)] mechanism and (b) end-effector.[22]

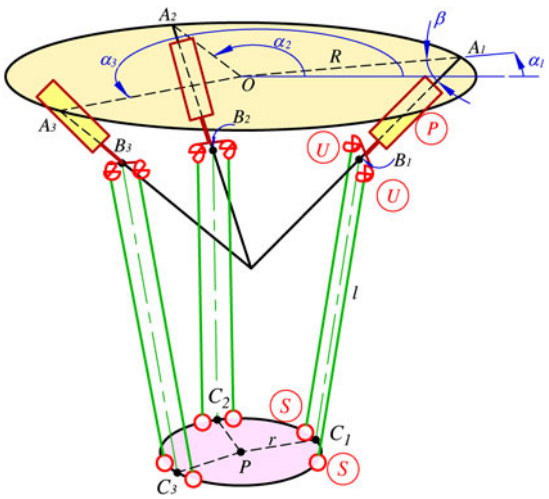


Fig. 2. Geometry the 3-[P2(US)] mechanism.

https://doi.org/10.1017/S0263574718001273 Published online by Cambridge University Press

Table I. Geometric parameters.

Parameters	**Value**
α_i	$(i-1)\times 120^\circ$
β	40°
r	28 mm
R	325 mm
l	340 mm
$m_p,\ m_e$	0.5 kg
m_l	0.2 kg

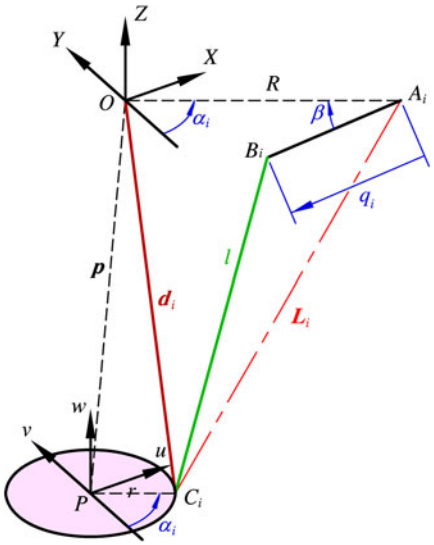


Fig. 3. Kinematic variables of one of the limbs.

are constructed in each limb in a way that only three translational motions are possible for the end-effector.

Geometric and physical parameters of the robot are considered as follows in Table I. The physical setup of the mechanism has been constructed in a robotics lab. DOF analysis, using screw theory, shows three pure translational DOF for the mechanism. Additionally, practical inspection of the physical setup and also motion simulation in ADAMS software show same result again. The main idea is the utilization of parallelogram linkages in each limb of the mechanism that can serve pure translational motion of the end-effector. The angle of 40° for prismatic directions is optimized in order to achieve to larger workspace.

3. Kinematic Analysis

In this section, inverse kinematics, velocity analysis, and Jacobians of the mechanism are considered.

3.1. Inverse kinematics

In inverse kinematics, the goal is obtaining the actuators positions, given the end-effector position with respect to the fixed platform frame. Figure 3 demonstrates kinematic variables of a robot limb in which the end-effector position P is described in fixed platform (Frame O).

Referring to Fig. 3, the following vector relation can be written

$$\mathbf{L}_i = q_i \mathbf{e}_{A_iB_i} + l\mathbf{e}_{B_iC_i} \qquad (i = 1, 2, 3) \tag{1}$$

where $\mathbf{L}_i = \overrightarrow{A_iC_i}$, $\mathbf{e}_{A_iB_i}$, and $\mathbf{e}_{B_iC_i}$ are the unit vectors along A_iB_i and B_iC_i, respectively, and q_i represents the linear displacement of the ith actuator.

https://doi.org/10.1017/S0263574718001273 Published online by Cambridge University Press

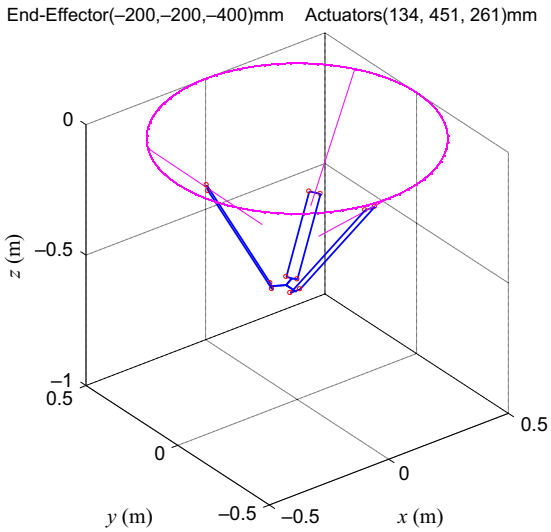


Fig. 4. An inverse kinematics solution for end-effector position of (−200, −200, −400) mm.

Through rewriting Eq. (1),

$$\left|\mathbf{L}_i - q_i \mathbf{e}_{A_iB_i}\right| = \left|l\mathbf{e}_{B_iC_i}\right| \tag{2}$$

Squaring both sides of (2) and rewriting,

$$\left|\mathbf{L}_i - q_i \mathbf{e}_{A_iB_i}\right|^2 = l^2 \tag{3}$$

Through simplification of Eq. (3) and solving it, inverse kinematics of the robot is obtained as Eq. (4).

$$q_i = \mathbf{L}_i^T \mathbf{e}_{A_iB_i} \pm \sqrt{\left(\mathbf{L}_i^T \mathbf{e}_{A_iB_i}\right)^2 - \mathbf{L}_i^T \mathbf{L}_i + l^2} \tag{4}$$

Noting that the moving frame *uvw* and the fixed frame *XYZ* remain parallel during the robot motion, directions of the vectors $\mathbf{r}_i$ and $\mathbf{R}_i$ remain the same so,

$$\begin{aligned}\mathbf{L}_i &= \mathbf{d}_i - \mathbf{R}_i = \mathbf{p} + \mathbf{r}_i - \mathbf{R}_i \\ &= \begin{pmatrix} x \\ y \\ z \end{pmatrix} + (r - R) \begin{pmatrix} \sin\alpha_i \\ -\cos\alpha_i \\ 0 \end{pmatrix}\end{aligned} \tag{5}$$

where $\mathbf{d}_i = \overrightarrow{OC_i}$, $\mathbf{R}_i = \overrightarrow{O_iA_i}$, $\mathbf{p} = \overrightarrow{OP}$, and $\mathbf{r}_i = \overrightarrow{PC_i}$. As shown in Eq. (4), in order to calculate actuator positions, given the coordination of mobile platform, two solutions exist. So there exist eight possible configurations for a given end-effector position $\mathbf{p}$. Investigating the obtained solutions, selecting only negative root leads to enhanced stiffness of the robot, because the three legs are inclined inward from top to bottom. Final equation is provided in Eq. (6) as follows:

$$q_i = \mathbf{L}_i^T \mathbf{e}_{A_iB_i} - \sqrt{\left(\mathbf{L}_i^T \mathbf{e}_{A_iB_i}\right)^2 - \mathbf{L}_i^T \mathbf{L}_i + l^2} \tag{6}$$

where

$$\mathbf{e}_{A_iB_i} = \begin{pmatrix} -\cos\beta\sin\alpha_i \\ \cos\beta\cos\alpha_i \\ -\sin\beta \end{pmatrix} \quad (i = 1, 2, 3) \tag{7}$$

A typical inverse kinematics solution for a given end-effector position is depicted in Fig. 4.

https://doi.org/10.1017/S0263574718001273 Published online by Cambridge University Press

3.2. Velocity analysis

Jacobian matrix relates joint coordinate space to Cartesian coordinate task space and also relates end-effector forces to actuators forces. By employing the Jacobian matrix, the end-effector velocities, singular configurations of the mechanism, and the robot workspace can be investigated. In order to obtain this matrix, the kinematic equations adopted in previous sections should be differentiated with respect to time. Defining

$$\dot{\mathbf{p}} = \begin{bmatrix} \dot{x} & \dot{y} & \dot{z} \end{bmatrix}^T \tag{8}$$

as the end-effector velocities and

$$\dot{\mathbf{q}} = \begin{bmatrix} \dot{q}_1 & \dot{q}_2 & \dot{q}_3 \end{bmatrix}^T \tag{9}$$

as the actuator velocities, the Jacobian elements in the following equation may be established.

$$\dot{\mathbf{p}} = \mathbf{J}\dot{\mathbf{q}} \tag{10}$$

Equation (10) is known as forward velocity kinematics of the mechanism. Another way to obtain the Jacobian is to derive it directly from the following velocity equation:

$$\dot{\mathbf{p}} = \mathbf{v}_{B_i} = \dot{q}_i \mathbf{e}_{A_i B_i} + \boldsymbol{\omega}_i \times l\mathbf{e}_{B_i C_i} \quad (i = 1, 2, 3) \tag{11}$$

where $\boldsymbol{\omega}_i$ is the angular velocity of two parallel rods in the ith limb which can be eliminated by dot multiplying both sides of Eq. (11) with $\mathbf{e}_{B_i C_i}$.

$$\dot{\mathbf{p}}.\mathbf{e}_{B_i C_i} = \dot{q}_i \mathbf{e}_{A_i B_i}.\mathbf{e}_{B_i C_i} \quad (i = 1, 2, 3) \tag{12}$$

The three Eqs. (12) can be written in the following matrix form:

$$\mathbf{J}_p \dot{\mathbf{p}} = \mathbf{J}_q \dot{\mathbf{q}} \tag{13}$$

where

$$\mathbf{J}_p = \begin{bmatrix} \mathbf{e}_{B_1 C_1}^T \\ \mathbf{e}_{B_2 C_2}^T \\ \mathbf{e}_{B_3 C_3}^T \end{bmatrix} \tag{14}$$

$$\mathbf{J}_q = diag \left[\mathbf{e}_{A_1 B_1}.\mathbf{e}_{B_1 C_1} \mathbf{e}_{A_2 B_2}.\mathbf{e}_{B_2 C_2} \mathbf{e}_{A_3 B_3}.\mathbf{e}_{B_3 C_3} \right]$$

Consequently,

$$\mathbf{J} = \mathbf{J}_p^{-1} \mathbf{J}_q \tag{15}$$

According to the limitations on the motions of robot joints, which are measured on the physical setup, the reachable kinematic workspace points were obtained numerically by try and error. Additionally, singular configurations were checked by the properties of Jacobian matrix and dynamic workspace was determined. So all the points used in dynamic simulations were selected in the kinematic and dynamic workspace.

4. Dynamic Modeling

In order to extract dynamic model of the mechanism, Lagrange and virtual work methods are used.

4.1. Lagrange equations

In this section, the dynamics of the robot is investigated and the dynamic model of the mechanism is derived based on the kinematic modeling which was presented in previous section. To drive the dynamic model of the robot, the Lagrange method is used. Since there are constraints on generalized coordinates in the parallel mechanism, the general formulation of constrained Lagrange equations with Lagrange multipliers is considered as follows:

https://doi.org/10.1017/S0263574718001273 Published online by Cambridge University Press

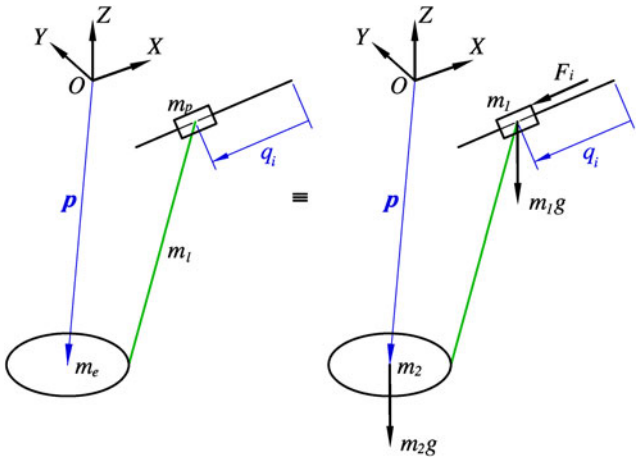


Fig. 5. Mass elements of one of the limbs.

$$\frac{d}{dt}\left(\frac{\partial L}{\partial \dot{\theta}_j}\right)-\frac{\partial L}{\partial \theta_j}=Q_j+\sum_{i=1}^{k}\lambda_i\frac{\partial \Gamma_i}{\partial \theta_j},\ (j=1,\ ...,\ 6) \tag{16}$$

where θ_j is the jth generalized coordinate and Q_j is the corresponding generalized force. Also, λ_i, Γ_i, and k indicate the Lagrange multipliers, constraint functions, and the number of system constraints, respectively. Generalized coordinates to describe the system are

$$\boldsymbol{\theta}=\begin{bmatrix}\mathbf{q}\\ \mathbf{p}\end{bmatrix} \tag{17}$$

where $\mathbf{q}$ includes the positions of actuators (prismatic joint variables) and $\mathbf{p}$ includes the end-effector position components. The general formulation of Lagrangian function is written as

$$L(\boldsymbol{\theta},\dot{\boldsymbol{\theta}})=K(\boldsymbol{\theta},\dot{\boldsymbol{\theta}})-U(\boldsymbol{\theta}) \tag{18}$$

where K and U are the kinetic and potential energies of the robot, respectively. According to Fig. 5, it is supposed that the masses of six connecting rods are equal and concentrated at rod ends, neglecting their rotational inertia.

The kinetic energy term of the mechanism can be written as

$$K=\frac{1}{2}m_1\left(\dot{q}_1^2+\dot{q}_2^2+\dot{q}_3^2\right)+\frac{1}{2}m_2\left(\dot{x}^2+\dot{y}^2+\dot{z}^2\right) \tag{19}$$

The masses concentrated at each prismatic joint and the moving platform are introduced as

$$m_1=m_p+\frac{m_l}{2}\qquad m_2=m_e+3\left(\frac{m_l}{2}\right) \tag{20}$$

where m_e, m_l, and m_p are the masses of end-effector, two connecting rods, and actuators piston, respectively. Thus four concentrated moving masses constitute the kinetic energy (three masses of m_1 associated to sliding parts of actuators and one mass of m_2 associated to moving platform).

Now, the potential energy of the mechanism can be written as

$$U=-m_1 g\sin\beta\,(q_1+q_2+q_3)+m_2 g\,z \tag{21}$$

where β is the angle of prismatic joints direction. Substituting Eqs. (19) and (21) in Eq. (18) gives the Lagrangian function as follows:

$$\begin{aligned}L=&\tfrac{1}{2}m_1\left(\dot{q}_1^2+\dot{q}_2^2+\dot{q}_3^2\right)+\tfrac{1}{2}m_2\left(\dot{x}^2+\dot{y}^2+\dot{z}^2\right)\\&-\left[m_2 g z-m_1 g\sin\beta(q_1+q_2+q_3)\right]\end{aligned} \tag{22}$$

https://doi.org/10.1017/S0263574718001273 Published online by Cambridge University Press

The constraint equations can be adopted from Eq. (6) as

$$\begin{aligned}\Gamma_i = &(x - R\sin\alpha_i + r\sin\alpha_i + q_i\cos\beta\sin\alpha_i)^2 \\ &+ (y + R\cos\alpha_i - r\cos\alpha_i - q_i\cos\beta\cos\alpha_i)^2 \\ &+ (z + q_i\sin\beta)^2 - l^2 = 0 \qquad (i = 1, 2, 3)\end{aligned} \tag{23}$$

Taking partial derivatives of constraint equations used in Lagrange equations and then substituting in Eq. (16), the equations of motion derived as follows:

$$\begin{aligned}&m_1\ddot{q}_i - \lambda_i(2\cos\beta\sin\alpha_i(x - y + (\cos\alpha_i + \sin\alpha_i) \\ &(r - R + q_i\cos\beta)) + 2\sin\beta(z + q_i\sin\beta)) \\ &\quad - m_1 g\sin\beta = F_i \qquad (i = 1, 2, 3)\end{aligned} \tag{24}$$

$$m_2\ddot{x} - \sum_{j=1}^{3} 2\lambda_j\left\{x + \left[(r - R) + q_j\cos\beta\right]\cos\alpha_j\right\} = 0 \tag{25}$$

$$m_2\ddot{y} - \sum_{j=1}^{3} 2\lambda_j\left\{y + \left[(r - R) + q_j\cos\beta\right]\sin\alpha_j\right\} = 0 \tag{26}$$

$$m_2\ddot{z} + m_2 g - \sum_{j=1}^{3} 2\lambda_j\left\{z + q_j\sin\beta\right\} = 0 \tag{27}$$

There are nine unknown variables including actuator coordinates (q_i), end-effector coordinates (x, y, z), and Lagrange multipliers (λ_i) in the six differential equations. In order to solve the differential equations of motion, three other equations should be considered. These three equations are derived by twice differentiation of constraint equations (23) with respect to time as follows:

$$\begin{aligned}&(q_i + (r - R)\cos\beta + z\sin\beta \\ &\quad + x\cos\beta\sin\alpha_i - 2y\cos\beta\cos\alpha_i)\ddot{q}_i \\ &\quad + (x - (r - R) + q_i\cos\beta)\sin\alpha_i\ddot{x} \\ &\quad + (y - (r - R) - q_i\cos\beta)\cos\alpha_i\ddot{y} \\ &\quad + (z + q_i\sin\beta)\ddot{z} + \dot{x}^2 + \dot{y}^2 + \dot{z}^2 \\ &\quad + 2\dot{q}_i\dot{x}\cos\beta\sin\alpha_i - 2\dot{q}_i\dot{y}\cos\beta\cos\alpha_i \\ &\quad + 2\dot{q}_i\dot{z}\sin\beta = 0 \qquad (i = 1, 2, 3)\end{aligned} \tag{28}$$

Solving nine differential equations gives the nine unknown variables in each time step. Lagrange multipliers may be eliminated using Eqs. (25)–(27) from Lagrange equations. Substituting obtained values of Lagrange multipliers into remaining Lagrange equations and also after some mathematical simplification, matrix form of equations of motion is as follows:

$$\mathbf{M}(\boldsymbol{\theta})\ddot{\boldsymbol{\theta}} + \mathbf{C}(\boldsymbol{\theta}, \dot{\boldsymbol{\theta}})\dot{\boldsymbol{\theta}} + \mathbf{G}(\boldsymbol{\theta}) = \overline{\mathbf{F}} \tag{29}$$

Partitioned form of the equations is written as

$$\begin{aligned}&\begin{bmatrix}\mathbf{M_{qq}} & \mathbf{M_{pq}} \\ \mathbf{M_{qp}} & \mathbf{M_{pp}}\end{bmatrix}\begin{bmatrix}\ddot{\mathbf{q}} \\ \ddot{\mathbf{p}}\end{bmatrix} + \begin{bmatrix}\mathbf{C_{qq}} & \mathbf{C_{pq}} \\ \mathbf{C_{qp}} & \mathbf{C_{pp}}\end{bmatrix}\begin{bmatrix}\dot{\mathbf{q}} \\ \dot{\mathbf{p}}\end{bmatrix} \\ &\quad + \begin{bmatrix}\mathbf{G_q} \\ \mathbf{G_p}\end{bmatrix} = \begin{bmatrix}\mathbf{F} \\ \mathbf{0}\end{bmatrix}\end{aligned} \tag{30}$$

4.2. Inverse dynamics

The objective of inverse dynamics, which can be used in robot control, is to calculate the actuator forces given a desired path for the end-effector. Desired trajectory and motion of the end-effector are given in terms of desired position vector $\mathbf{p}(t)$ and its time derivatives $\dot{\mathbf{p}}(t)$ and $\ddot{\mathbf{p}}(t)$ as functions of time. Using inverse kinematics of position and velocity, $\mathbf{q}$ and $\dot{\mathbf{q}}$ are obtained. Referring to Eq. (30):

$$\mathbf{M_{pq}}\ddot{\mathbf{q}} + \mathbf{M_{pp}}\ddot{\mathbf{p}} + \mathbf{C_{pq}}\dot{\mathbf{q}} + \mathbf{C_{pp}}\dot{\mathbf{p}} + \mathbf{G_p} = \mathbf{0} \tag{31}$$

https://doi.org/10.1017/S0263574718001273 Published online by Cambridge University Press

Equation (31) can be rewritten as follows:

$$\ddot{\mathbf{q}} = -\mathbf{M}_{\mathbf{pq}}^{-1}\left[\mathbf{M}_{\mathbf{pp}}\ddot{\mathbf{p}} + \mathbf{C}_{\mathbf{pq}}\dot{\mathbf{q}} + \mathbf{C}_{\mathbf{pp}}\dot{\mathbf{p}} + \mathbf{G}_{\mathbf{p}}\right] \tag{32}$$

Actually, Eq. (32) is the inverse kinematics of acceleration. Substituting $\ddot{\mathbf{q}}$ in Eq. (33), actuating forces are determined.

$$\mathbf{F} = \mathbf{M}_{\mathbf{qq}}\ddot{\mathbf{q}} + \mathbf{M}_{\mathbf{qp}}\ddot{\mathbf{p}} + \mathbf{C}_{\mathbf{qq}}\dot{\mathbf{q}} + \mathbf{C}_{\mathbf{qp}}\dot{\mathbf{p}} + \mathbf{G}_{\mathbf{q}} \tag{33}$$

4.3. Forward dynamics

The objective of forward dynamics, which is used in motion simulations, is to calculate the trajectory of the robot ($\mathbf{p}(t)$) given the actuator forces and initial conditions of the mechanism. Using Eq. (29):

$$\ddot{\boldsymbol{\theta}} = -\mathbf{M}^{-1}(\boldsymbol{\theta})\left[\overline{\mathbf{F}}(\mathbf{t}) - \mathbf{C}(\boldsymbol{\theta}, \dot{\boldsymbol{\theta}}) - \mathbf{G}(\boldsymbol{\theta})\right] \tag{34}$$

The nonlinear system of differential equations (34) can be solved using a numerical method that provides values of $\boldsymbol{\theta}(t) = \left[\mathbf{q}^T(t)\ \mathbf{p}^T(t)\right]^T$ in simulations.

4.3.1. Computational algorithm of Lagrange's method. A computational algorithm for solving the derived dynamic model of the robot based on Lagrange method is as follows:

(1) Determine the desired motion for the end-effector and define $\mathbf{p_d}, \dot{\mathbf{p}}_\mathbf{d}, \ddot{\mathbf{p}}_\mathbf{d}$.
(2) Solve inverse kinematics equations (4), (10), and (40) and compute $\mathbf{q_d}, \dot{\mathbf{q}}_\mathbf{d}, \ddot{\mathbf{q}}_\mathbf{d}$.
(3) Solve inverse dynamics equation (33) and find actuating forces $\mathbf{F}$.
(4) Determine the initial conditions of the end-effector $\mathbf{p}_0$, $\dot{\mathbf{p}}_0$.
(5) Solve inverse kinematics equations (4) and (10) and find $\mathbf{q}_0$, $\dot{\mathbf{q}}_0$.
(6) Constitute $\boldsymbol{\theta}$, $\dot{\boldsymbol{\theta}}$ using Eq. (17).
(7) Solve forward dynamics equation (34) and find $\ddot{\boldsymbol{\theta}}$.
(8) Using numerical integration algorithm (e.g., Runge–Kutta method) to find $\boldsymbol{\theta}$, $\dot{\boldsymbol{\theta}}$ and go to step 7.

4.4. Virtual work modeling

Equations of motion are derived here using the principle of virtual work which has some advantage over Lagrange equations. The principle can be written as[23]

$$\delta W_F + \delta W_g + \delta W_I = 0 \tag{35}$$

which shows the sum of virtual works done by actuator forces, weight, and inertial forces. So the equation can be written as

$$\mathbf{F}^T\delta\mathbf{q} + \mathbf{G}_1^T\delta\mathbf{q} + \mathbf{G}_2^T\delta\mathbf{p} + \mathbf{f}_1^T\delta\mathbf{q} + \mathbf{f}_2^T\delta\mathbf{p} = \mathbf{0} \tag{36}$$

where

$$\begin{aligned}
\mathbf{F} &= \left[F_1\ F_2\ F_3\right]^T \\
\mathbf{G}_1 &= \left[m_1 g \sin\beta\ m_1 g \sin\beta\ m_1 g \sin\beta\right]^T \\
\mathbf{G}_2 &= -\left[0\ 0\ m_2 g\right]^T \\
\mathbf{f}_1 &= -\left[m_1\ddot{q}_1\ m_1\ddot{q}_2\ m_1\ddot{q}_3\right]^T \\
\mathbf{f}_2 &= -\left[m_2\ddot{x}\ m_2\ddot{y}\ m_2\ddot{z}\right]^T \\
\delta\mathbf{q} &= \left[\delta q_1\ \delta q_2\ \delta q_3\right]^T \\
\delta\mathbf{p} &= \left[\delta x\ \delta y\ \delta z\right]^T
\end{aligned} \tag{37}$$

Free body diagram of one of the limbs depicting actuating, gravitation, and inertial forces and virtual displacements is illustrated in Fig. 6.

From Eq. (10), there is a relation between virtual displacements as

$$\delta\mathbf{p} = \mathbf{J}\delta\mathbf{q}. \tag{38}$$

https://doi.org/10.1017/S0263574718001273 Published online by Cambridge University Press

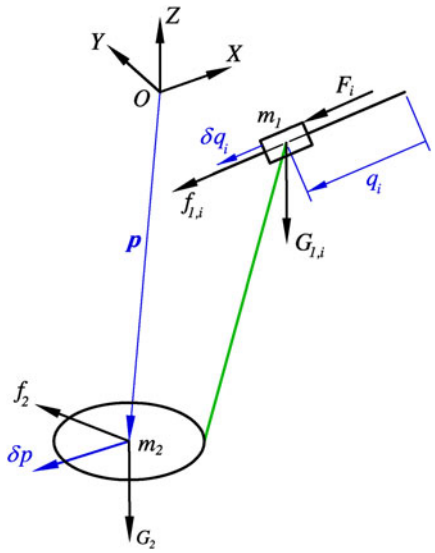


Fig. 6. Free body diagram of one of the limbs.

Substituting (38) in (36) yields

$$\left(\mathbf{F}^T + \mathbf{G}_1^T + \mathbf{G}_2\mathbf{J} + \mathbf{f}_1^T + \mathbf{f}_2^T\mathbf{J}\right)\delta\mathbf{q} = \mathbf{0} \tag{39}$$

Since this equation holds for any virtual displacement $\delta\mathbf{q}$, we can get

$$\mathbf{F}^T + \mathbf{G}_1^T + \mathbf{G}_2\mathbf{J} + \mathbf{f}_1^T + \mathbf{f}_2^T\mathbf{J} = \mathbf{0} \tag{40}$$

Taking the transpose of Eq. (40) and rearranging it yields

$$\mathbf{F} = -\mathbf{G_1} - \mathbf{J^T G_2} - \mathbf{f_1} - \mathbf{J}^T\mathbf{f_2} \tag{41}$$

Substituting the inertial forces into Eq. (41) yields

$$\mathbf{F} = -\mathbf{G_1} - \mathbf{J^T G_2} + \mathbf{M_q}\ddot{\mathbf{q}} + \mathbf{J^T M_p}\ddot{\mathbf{p}} \tag{42}$$

where

$$\begin{aligned}\mathbf{M}_q &= diag\,\{m_1, m_1, m_1\}\\ \mathbf{M}_p &= diag\,\{m_2, m_2, m_2\}\end{aligned} \tag{43}$$

Differentiating Eq. (10) with respect to time,

$$\ddot{\mathbf{p}} = \dot{\mathbf{J}}\dot{\mathbf{q}} + \mathbf{J}\ddot{\mathbf{q}} \tag{44}$$

which yields

$$\ddot{\mathbf{q}} = \mathbf{J}^{-1}(\ddot{\mathbf{p}} - \dot{\mathbf{J}}\dot{\mathbf{q}}) \tag{45}$$

Substituting (45) in (42) yields

$$\begin{aligned}\ddot{\mathbf{p}} = &\left(\mathbf{M_q J}^{-1} + \mathbf{J^T M_p}\right)^{-1}\\ &\left[\mathbf{F} + \mathbf{G_1} + \mathbf{J^T G_2} + \mathbf{M_q J}^{-1}\dot{\mathbf{J}}\dot{\mathbf{q}}\right]\end{aligned} \tag{46}$$

Equations (45) and (46) are equivalent to (31) and (33) which can be used in inverse dynamics and simulation of the mechanism. Implementation of Eqs. (45) and (46) in numerical simulations needs a less computational effort in comparison with Eqs. (31) and (33), due to not introducing any multipliers and then eliminating them, and so this approach is more suitable for real-time control. Comparison of computation times of the two models (coming from Lagrange's method and the principle of virtual work) is introduced through numerical simulations in the following sections.

https://doi.org/10.1017/S0263574718001273 Published online by Cambridge University Press

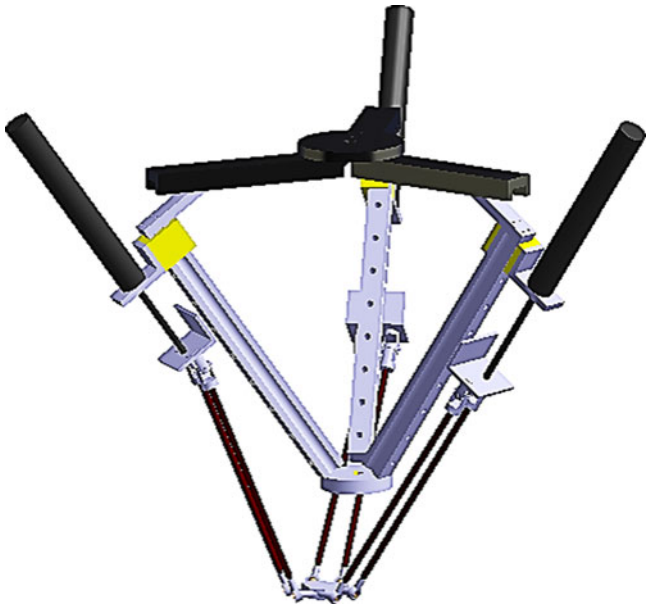


Fig. 7. ADAMS model of the mechanism.

4.4.1. Computational algorithm of principle of virtual work method. A computational algorithm for solving the derived dynamic model of the robot based on the principle of virtual work is as follows:

(1) Determine the desired motion of the end-effector and define $\mathbf{p_d}$, $\dot{\mathbf{p}}_\mathbf{d}$, $\ddot{\mathbf{p}}_\mathbf{d}$.
(2) Solve inverse kinematics equations (4), (10), and (53) and find $\mathbf{q_d}$, $\dot{\mathbf{q}}_\mathbf{d}$, $\ddot{\mathbf{q}}_\mathbf{d}$.
(3) Solve inverse dynamics equation (42) and find actuating forces $\mathbf{F}$.
(4) Determine the initial conditions of the end-effector $\mathbf{p}_0$, $\dot{\mathbf{p}}_0$.
(5) Solve inverse kinematics equations (4) and (10) and find $\mathbf{q}_0$, $\dot{\mathbf{q}}_0$.
(6) Solve inverse dynamics equations (45) and (46) and find $\ddot{\mathbf{p}}$, $\ddot{\mathbf{q}}$.
(7) Using numerical integration algorithm (e.g., Runge–Kutta method) to find $\mathbf{p}$, $\mathbf{q}$, $\dot{\mathbf{p}}$, $\dot{\mathbf{q}}$ and go to step 6.

5. Model Verification

A simulation is performed utilizing ADAMS software in order to verify correctness of the derived model and to study its sensitivity to simplifying assumptions adopted in the model. A schematic of the mechanism modeled in the software is depicted in Fig. 7. Three actuating forces of $10\cos(5t)$, $10\sin(4t)$, and $10\cos(5t)\sin(4t)$ are applied on the mechanism and its motion during 2 s is simulated. Motion curves of the end-effector are displayed in Fig. 8.

According to Fig. 8, assumption of two concentrated masses on the two ends of connecting rods has negligible effect on motion simulation.

6. Simulation Results

6.1. Case 1

In the first simulation, three equal harmonic actuating forces with amplitude of –19 N are considered as shown in Fig. 9. Negative sign means that the applied forces are in opposite directions to the downward positive direction assumed for actuators. The forces are applied half cycle in 1 s duration.

Using forward dynamics, with the initial position of (0, 0, –300 mm) and zero initial velocity for the end-effector, simulation results are shown in Figs. 10–12. Due to equal actuating forces and geometrical symmetry of the mechanism, three equal motions for the three actuators (prismatic joints) can be seen.

Also due to symmetry, the end-effector motion is expected only along the z-direction which can be seen in Fig. 11. At the beginning of motion when the mechanism weight dominates the actuators forces, the end-effector and prismatic joints move downward. Increasing the opposing forces of the

https://doi.org/10.1017/S0263574718001273 Published online by Cambridge University Press

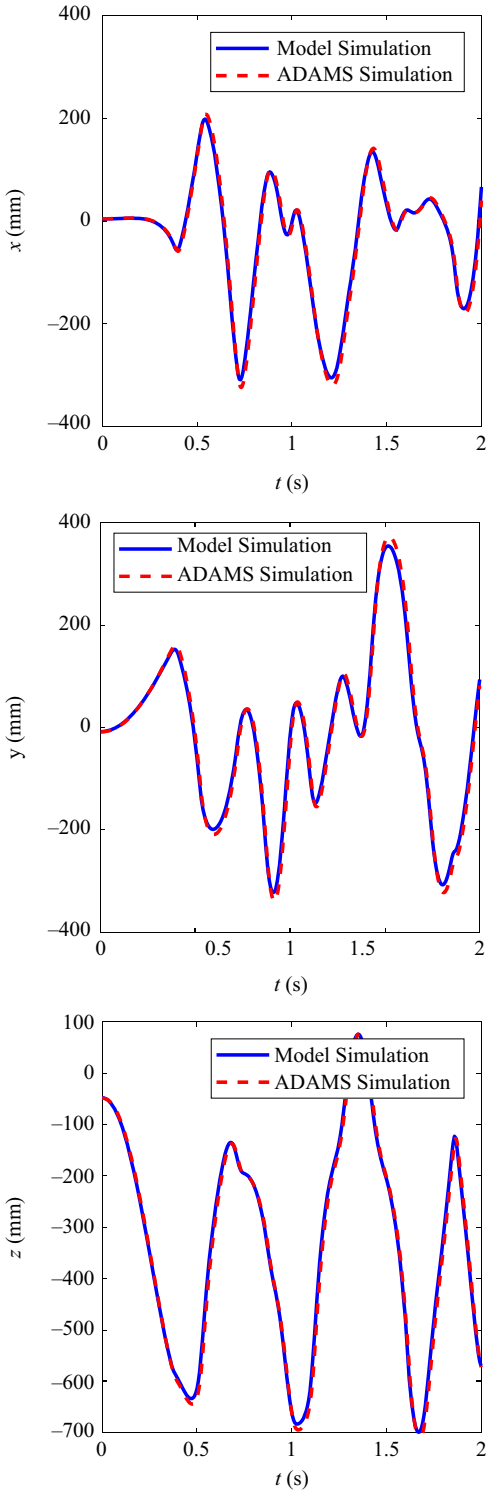


Fig. 8. Motion curves of the end-effector.

actuators, the motion is inverted and changes to upward. At the end of motion, by reducing the forces of actuators, the velocity is reduced and the mechanism prepares to move downward again.

Figure 12. shows the trajectory of the end-effector from two different views. Qualitative agreement of simulation results with expected motion verifies the validity of the derived model.

The total non-conservative work done by actuators (W_a) in four intervals of motion and the corresponding changes in mechanical energy are computed and displayed in Table II.

https://doi.org/10.1017/S0263574718001273 Published online by Cambridge University Press

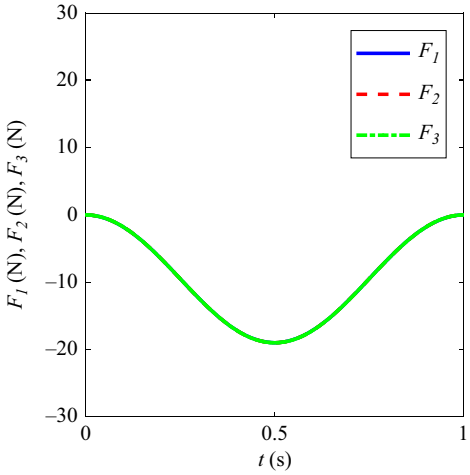


Fig. 9. The forces of actuators.

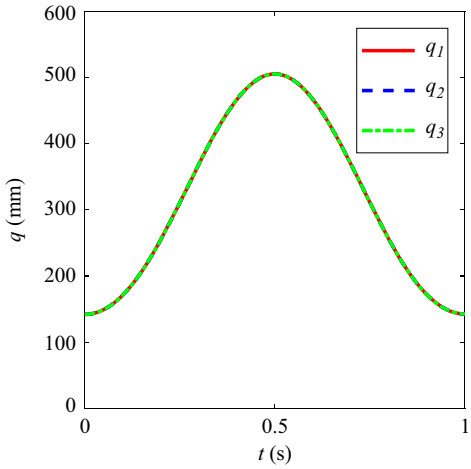


Fig. 10. Motion curve of actuators.

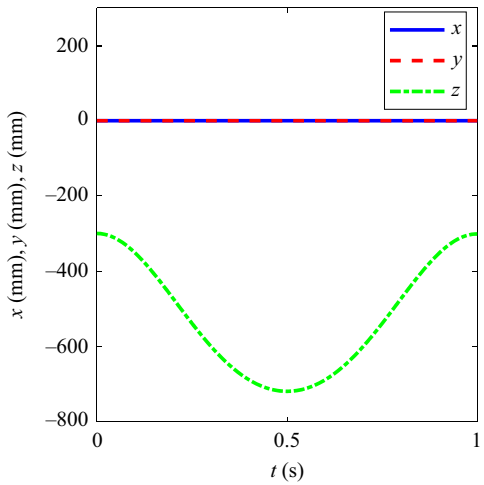


Fig. 11. Motion of the end-effector.

https://doi.org/10.1017/S0263574718001273 Published online by Cambridge University Press

Table II. Actuator works and mechanical energy increments.

Interval(s)	$W_a(J)$	$\Delta K + \Delta U\ (J)$	**Difference (%)**
0.00–0.25	−2.516	−2.492	0.96
0.25–0.50	−8.39	−8.363	0.32
0.50–0.75	8.315	8.342	0.33
0.75–1.00	2.465	2.489	0.98

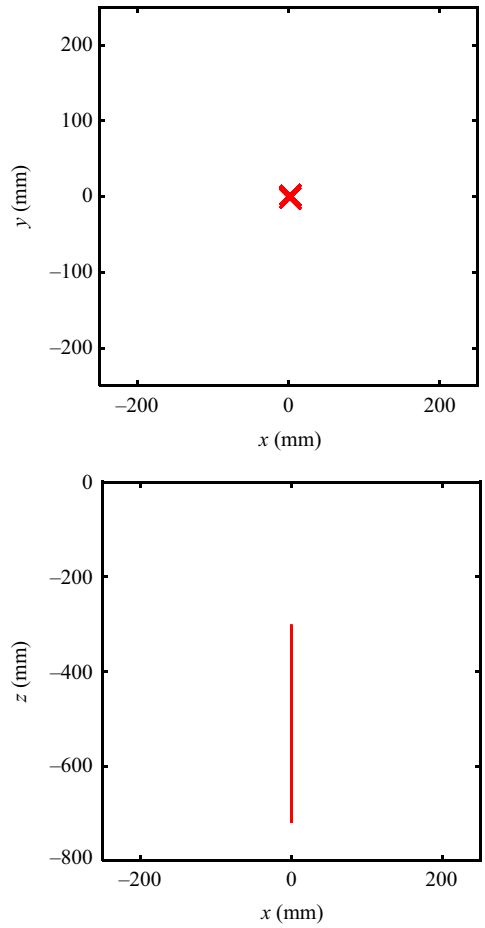


Fig. 12. Trajectory of end-effector.

There are small differences between actuator works and mechanical energy changes which are related to numerical simulation errors. Results verify the validity of the derived equations of motion, quantitatively.

6.2. Case 2

In the second simulation, two equal harmonic forces with amplitude of –24 N are considered for two actuators, and zero force is considered for the third as depicted in Fig. 13.

Using forward dynamics, with the initial position of (0, 0, –300 mm) and zero initial velocity for the end-effector, simulation results are shown in Figs. 14–16. Again, due to the two equal actuating forces and geometrical symmetry of the mechanism, two similar motions are seen for the actuators 1 and 2, and a different motion is seen for the actuator 3 in Fig. 14.

According to asymmetry of forces in the three actuators, end-effector motion is expected to exist along all the three axes which can be seen in Fig. 15.

Figure 16 shows the trajectory of end-effector in two views. Domination of weight force in the beginning and end of motion duration, and that of actuating forces in the middle is also seen here.

https://doi.org/10.1017/S0263574718001273 Published online by Cambridge University Press

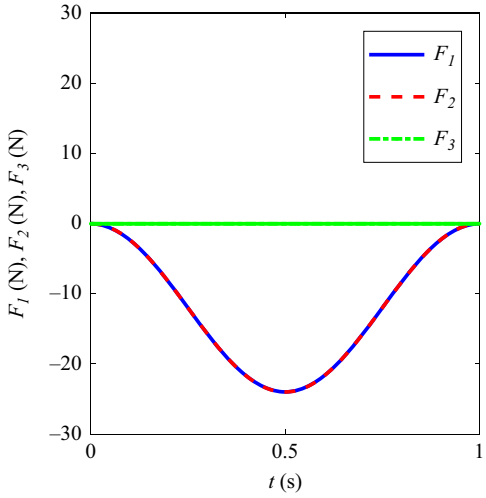


Fig. 13. Applying forces of actuators.

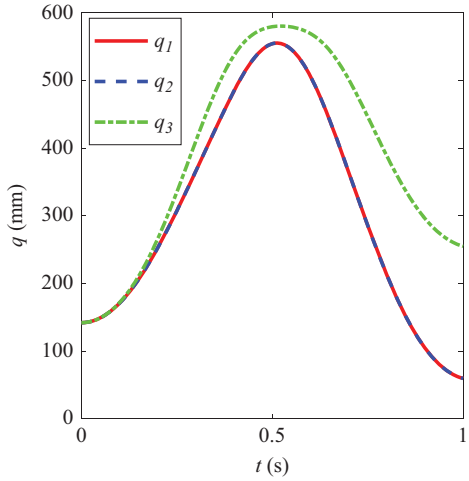


Fig. 14. Curves of the actuator motions.

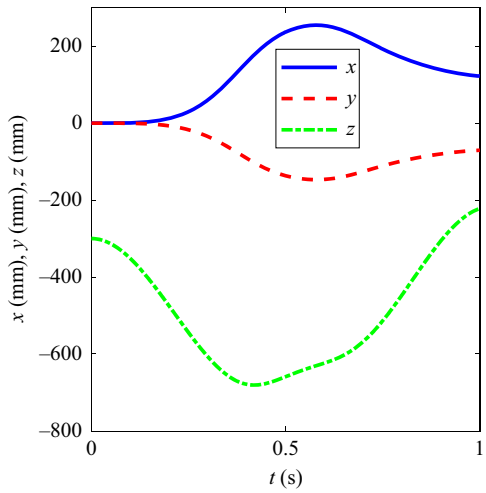


Fig. 15. End-effector motions.

https://doi.org/10.1017/S0263574718001273 Published online by Cambridge University Press

Table III. Actuators works and mechanical energy increments.

Interval(s)	$W_a(J)$	$\Delta K + \Delta U\ (J)$	**Difference (%)**
0.00–0.25	−2.072	−2.052	0.96
0.25–0.50	−9.34	−9.313	0.29
0.50–0.75	9.656	9.688	0.33
0.75–1.00	2.709	2.736	0.98

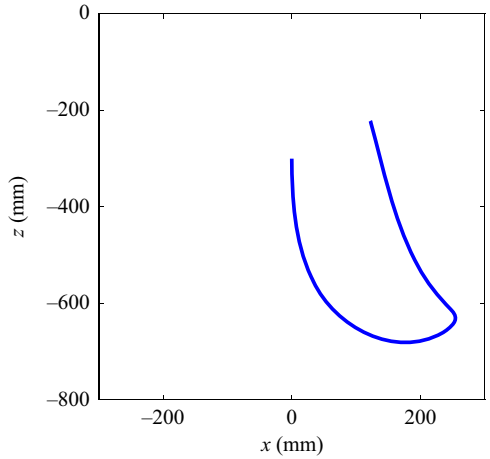


Fig. 16. End-effector trajectory.

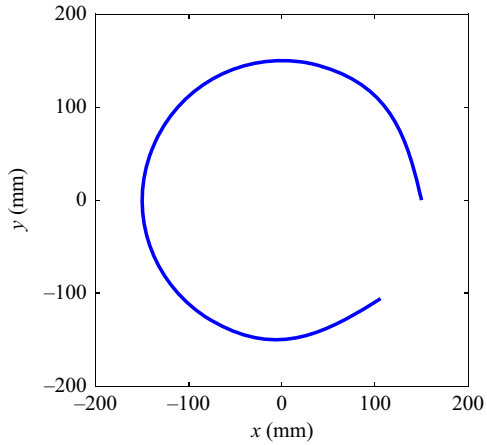


Fig. 17. Preferred trajectory for end-effector.

Because of equality of forces in two actuators and zero initial velocity, straight motion in horizontal plane is expected. Also, locating the two actuators in angles of –90° and 30° relative to the x-axis verifies the observed direction in horizontal plane.

The total actuators work in four intervals of motion and the corresponding changes of mechanical energy are again displayed in Table III.

6.3. Case 3

In the third simulation, a circular path with radius of 150 mm at elevation of –300 mm is considered for the end-effector which is shown in Fig. 17. Motion planning of the robot is performed by determining eight accuracy points and cubic spline interpolation of them with respect to time in duration of 3.5 s.

Curves for the end-effector motion with respect to time based on spline interpolation are shown in Fig. 18.

https://doi.org/10.1017/S0263574718001273 Published online by Cambridge University Press

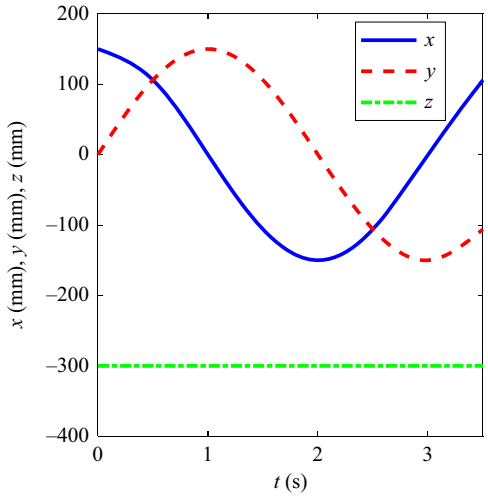


Fig. 18. Motion curves of end-effector.

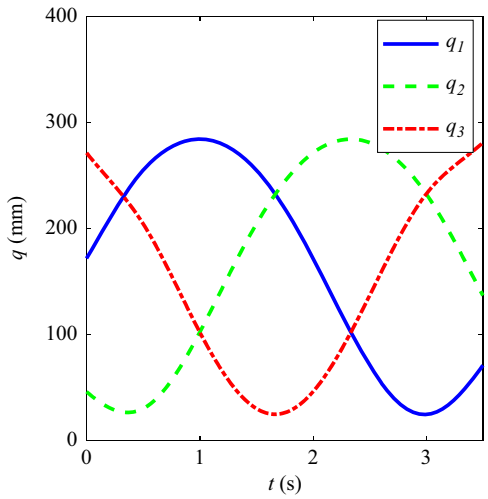


Fig. 19. Motion curves of actuators.

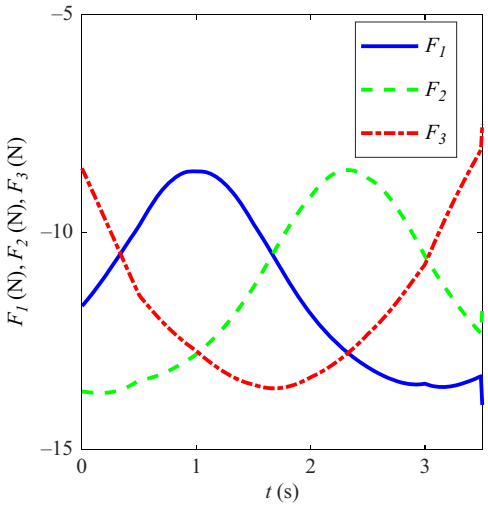


Fig. 20. Computed forces of actuators.

https://doi.org/10.1017/S0263574718001273 Published online by Cambridge University Press

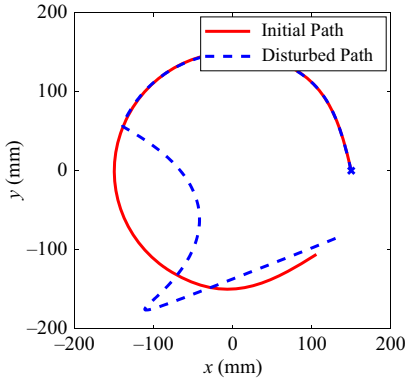


Fig. 21. Trajectory of the end-effector with and without disturbing impulse.

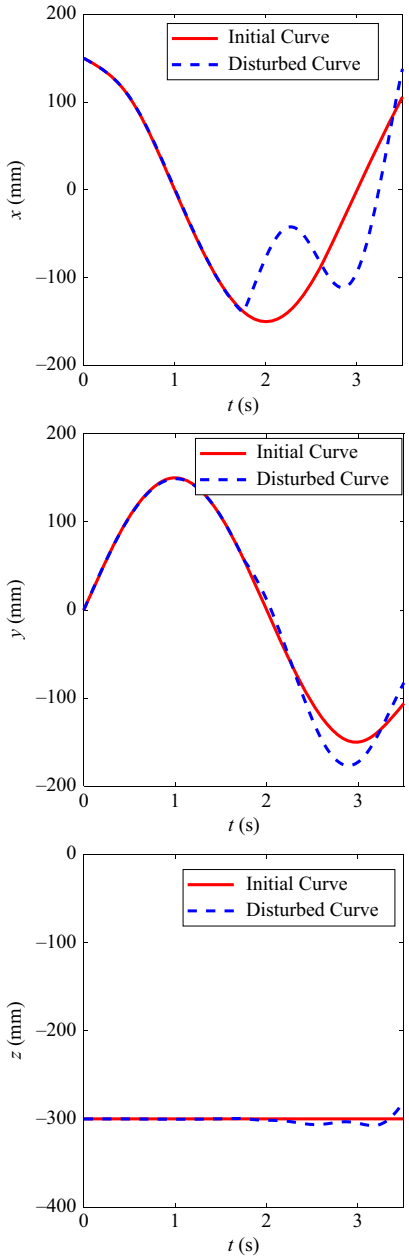


Fig. 22. Motion curves of the end-effector with and without disturbing impulse.

https://doi.org/10.1017/S0263574718001273 Published online by Cambridge University Press

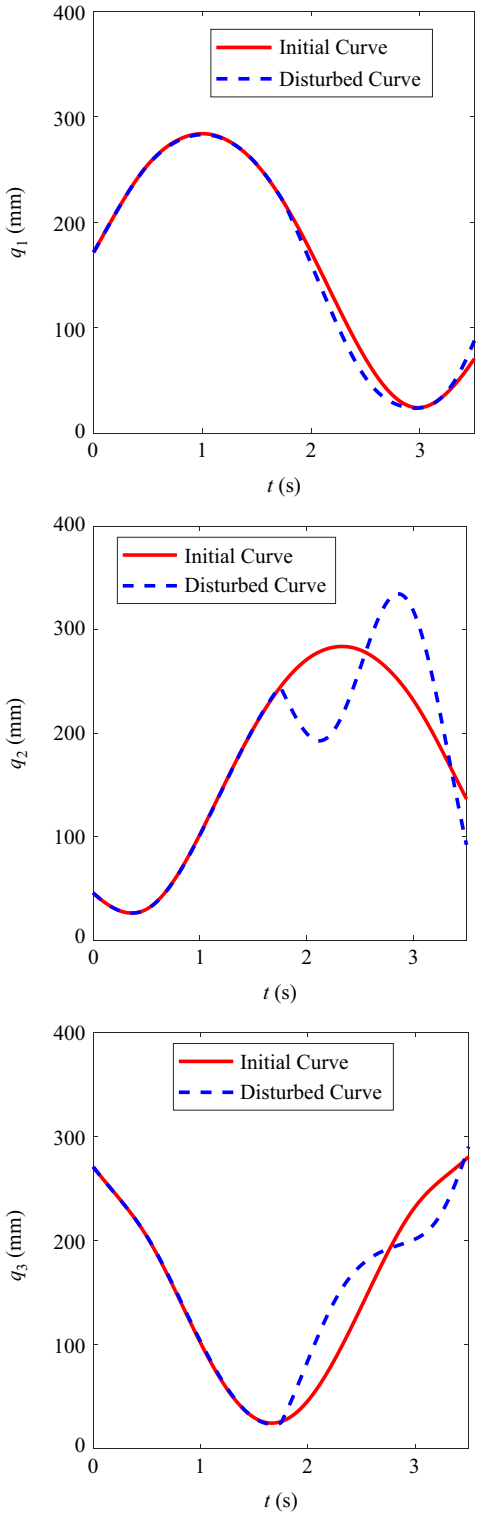


Fig. 23. Motion curves of actuators with and without disturbing impulse.

Using inverse kinematics, the motion curves for three actuators (prismatic joints) are obtained and depicted in Fig. 19.

Using inverse dynamics, the values of required forces in the actuators are computed for creating the desired path and shown in Fig. 20.

Implementing forward dynamics, the desired circular trajectory will be created by applying the computed actuator forces in the motion simulation.

https://doi.org/10.1017/S0263574718001273 Published online by Cambridge University Press

Table IV. Computation times of simulation of the two models for three cases.

Case	Model by Lagrange's method (s)	Model by principle of virtual work (s)	Reduction percent (%)
1	0.0826	0.069	19.710
2	0.089	0.072	23.611
3	0.313	0.257	21.790

Another simulation is performed considering a disturbing impulse equal to 0.585 N · s applying at t = 1.75 s in x-direction to the end-effector. A force of F = 50 N is considered to be exerted on the end-effector in a duration of $\Delta t = 0.0117$ s. Simulation results of forward dynamics considering the disturbing impulse are depicted in Figs. 21–23.

As can be seen, in the beginning of motion, before applying the impulse the mechanism moves on the initial desired trajectory. Due to the exertion of the disturbing impulse, the end-effector deviates from initial curve along x-direction and some oscillation is observed around the initial path which qualitatively verifies the expected motion.

The total linear momentum of the mechanism in x-direction is calculated immediately before and after applying the impulse of $F\Delta t = 0.585\,\mathrm{N}\cdot\mathrm{s}$. The linear momentum in x-direction can be determined as

$$\begin{aligned} P_x &= m_2 v_{\text{end-effector},x} + \sum_{i=1}^{3} m_1 v_{\text{piston},x} \\ &= m_2 \dot{x} - m_1 \sin\beta \sum_{i=1}^{3} \dot{q}_i \sin\alpha_i \end{aligned} \tag{47}$$

The change of linear momentum is computed as

$$\Delta P_x = P_x|_{t=1.75\,\mathrm{s}+\Delta t} - P_x|_{t=1.75\,\mathrm{s}} = 0.551\,\mathrm{kg}\frac{\mathrm{m}}{\mathrm{s}} \tag{48}$$

So, the total impulse in x-direction is approximately equal to the total momentum of the robot in x-direction. The value shows a slight difference from the applied impulse, and the difference is due to simplifying assumptions in computing the total impulse.

Computation times of simulations of the two derived models are compared in Table IV for the three simulation cases. Improvement of about 20% in computation times, for the model derived using the principle of virtual work, shows relative effectiveness of the model.

7. Conclusion

In this paper, a novel type of parallel robot with three translational DOF is studied. Inverse kinematic equations are extracted based on the robot geometry in order to be used in robot simulations. Derivation of kinematic equations which relate end-effector position to actuators positions is performed using constraint equations of the parallel mechanism. Velocity equations are derived by differentiation of position equations with respect to time, and velocity kinematics is described using Jacobian matrices. Dynamic modeling of the parallel mechanism is investigated and equations of motion are derived by Lagrange approach. First, six equations of motion are derived based on the Lagrangian of the system and Lagrange multipliers. Then, the second three equations are used to eliminate the Lagrange multipliers. Reduced dynamic equations of the robot, which consist of three remaining Lagrange equations and second derivative of three constraint equations, are represented in a partitioned matrix form. Inverse and forward dynamics of the mechanism are described using the derived matrix equation. Dynamic modeling is also done using the principle of virtual work which has some simplicity and less computation effort and is suitable for real-time control. Three simulations are performed by implementation of the kinematic and dynamic models. The numerical results show good agreement with expected qualitative behavior of the mechanism under the applied actuator forces. Comparing the results with work and energy theorem in two cases and with impulse and momentum theorem in the third quantitatively verifies the validity of the derived equations of motion.

https://doi.org/10.1017/S0263574718001273 Published online by Cambridge University Press

References

1. J.-P. Merlet, *Parallel Robots* (Kluwer Academic Publishers, London, 2001).
2. B. Monsarrat and C. Gosselin, "Workspace analysis and optimal design of a 3-leg 6-DOF parallel platform mechanism," *IEEE Trans. Robot. Autom.* **19**, 954–966 (2003).
3. M. H. Dado, N. S. Al-Huniti and A. K. Eljabali, "Dynamic simulation model for mixed-loop planar robots with flexible joint drives," *Mech. Mach. Theory* **36**, 547–559 (2001).
4. A. Codourey and E. Burdet, "A Body-Oriented Method for Finding a Linear form of the Dynamic Equation of Fully Parallel Robots," *IEEE International Conference on Robotics and Automation*, Alberquerque, NM (1997).
5. G. Liu and Z. Li, "A unified geometric approach to modeling and control of constrained mechanical systems," *IEEE Trans. Robot. Autom.* **18**(4), 574–587 (2002).
6. X.-M. Niu, G. Q. Gao, X. J. Liu and Z. D. Bao, "Dynamics and control of a novel 3-DOF parallel manipulator with actuation redundancy," *Int. J. Autom. Comput.* **10**(6), 552–562 (2013).
7. W. Do and D. Yang, "Inverse dynamic analysis and simulation of a platform type of robot," *J. Robot. Syst.* **5**, 209–227 (1988).
8. C. Reboulet and T. Berthomieu, "Dynamic Models of a Six Degree of Freedom Parallel Manipulators," *Proceedings of the IEEE International Conference on Robotics and Automation*, Pisa, Italy (1991) pp. 1153–1157.
9. Z. Ji, "Dynamics decomposition for Stewart platforms," *ASME J. Mech.* **116**, 67–69 (1994).
10. X. Zhao, "Design, analysis, and control of a cable-driven parallel platform with a pneumatic muscle active support," *Robotica* **35**(4), 744–765 (2017).
11. Y. Zhao, "Dynamic performance evaluation for a 3U P S-P RU parallel robot," *Int. J. Adv. Robot. Syst.* **13**(5), 1729881416665235 (2016).
12. M. Özdemir, "Dynamic analysis of planar parallel robots considering singularities and different payloads," *Robot. Comput. Integr. Manufact.* **46**, 114–121 (2017).
13. J. Mo, Z.-F. Shao, L. Guan, F. Xie and X. Tang, "Dynamic performance analysis of the X4 high-speed pick-and-place parallel robot," *Robot. Comput. Integr. Manuf.* **46**, 48–57 (2017).
14. Y. Lu and Z. Dai, "Dynamics model of redundant hybrid manipulators connected in series by three or more different parallel manipulators with linear active legs," *Mech. Mach. Theory* **103**, 222–235 (2016).
15. S. Staicu, X.-J. Liu and J. Wang, "Inverse dynamics of the HALF parallel manipulator with revolute actuators," *Nonlinear Dyn*. **50**, 1–12 (2007).
16. L.-W. Tsai, "Solving the inverse dynamics of Stewart–Gough manipulator by the principle of virtual work," *J. Mech. Des.* **122**, 3–9 (2000).
17. J. Gallardo, J. Rico, A. Frisoli, D. Checcacci and M. Bergamasco, "Dynamics of parallel manipulators by means of screw theory," *Mech. Mach. Theory* **38**, 1113–1131 (2003).
18. S. Staicu and D. Zhang, "A novel dynamic modelling approach for parallel mechanisms analysis," *Robot. Comput. Integr. Manufact.* **24**(1), 167–172 (2008).
19. K. Miller, "Optimal design and modeling of spatial parallel manipulators," *Int. J. Robot. Res.* **23**, 127–140 (2004).
20. S. Staicu, "Dynamics modelling of a Stewart-based hybrid parallel robot," *Adv. Robot.* **29**(14), 929–938 (2015).
21. Y. Li and Q. Xu, "Kinematics and inverse dynamics analysis for a general 3-PRS spatial parallel mechanism," *Robotica* **23**(2), 219–229 (2005).
22. M. Mazare, M. Taghizadeh and M. R. Najafi, "Kinematic analysis and design of a novel 3-DOF translational parallel robot," *Int. J. Autom. Comput*. (2016). doi:10.1007/s11633-017-1066-y.
23. J. H. Ginsberg, *Advanced Engineering Dynamics* (Cambridge University Press, New York, NY, 1998).

https://doi.org/10.1017/S0263574718001273 Published online by Cambridge University Press